Acta Materialia 205 (2021) 116543

Contents lists available at ScienceDirect

Acta Materialia

journal homepage: www.elsevier.com/locate/actamat

Mesoscopic nature of serration behavior in high-Mn austenitic steel

Sukyoung Hwang[a,*], Myeong-heom Park[b,*], Yu Bai[a,*], Akinobu Shibata[a,b,c], Wenqi Mao[a], Hiroki Adachi[d], Masugu Sato[e], Nobuhiro Tsuji[a,b,*]

[a] Department of Materials Science and Engineering, Kyoto University, Yoshida-honmachi, Sakyo-ku, Kyoto 606-8501, Japan
[b] Elements Strategy Initiative for Structural Materials (ESISM), Kyoto University, Yoshida-honmachi, Sakyo-ku, Kyoto 606-8501, Japan
[c] National Institute for Materials Science (NIMS), 1-2-1 Sengen, Tsukuba 305-0047, Japan
[d] Department of Materials and Synchrotron Radiation Engineering, Graduate School of Engineering, University of Hyogo, Himeji 671–2280, Japan
[e] Japan Synchrotron Radiation Research Institute (JARSI), Sayo-gun, Hyogo 679–5198, Japan

ARTICLE INFO

Article history:
Received 18 June 2020
Revised 8 October 2020
Accepted 2 December 2020
Available online 8 December 2020

Keywords:
Deformation localization
Portevin–Le Chatelier (PLC) band
Digital image correlation (DIC)
In-situ synchrotron XRD
Work hardening

ABSTRACT

We have thoroughly clarified the mesoscopic nature of serration behavior in a high-Mn austenitic steel in connection with its characteristic localized deformation. A typical high-Mn steel, Fe-22Mn-0.6C (wt. %), with a face centered cubic (FCC) single-phase structure was used in the present study. After 4 cycles of repeated cold-rolling and annealing process, a specimen with a fully recrystallized microstructure having a mean grain size of 2.0 μm was obtained. The specimen was tensile tested at room temperature at an initial strain rate of 8.3×10^{-4} s^{-1}, during which the digital image correlation (DIC) technique was applied for analyzing local strain and strain-rate distributions in the specimen. Obtained results indicated that a unique strain localization behavior characterized by the formation, propagation and annihilation of deformation localized bands, so-called Portevin–Le Chatelier (PLC) bands, determined the global mechanical response appearing as serration on the stress-strain curve. In addition, the *in-situ* synchrotron XRD diffraction during the tensile test was utilized to understand what was happening in the material with respect to the PLC banding. Lattice strain of (200) plane nearly perpendicular to the tensile direction dropped when every PLC band passed through the beam position, which indicated a stress relaxation occurred inside the PLC band. At the same time, the dislocation density increased drastically when the PLC band passed the beam position, which described that the material was plastically deformed and work-hardened mostly within the PLC band. All the results obtained consistently explained the serration behavior in a mesoscopic scale. The serration behavior on the stress-strain curve totally corresponded to the formation, propagation and annihilation of the PLC band in the 22Mn-0.6C steel, and the localized deformation, i.e., the PLC banding, governed the characteristic strain hardening of the material.

1. Introduction

Over several decades, high-Mn austenitic steels have been widely studied because of their outstanding mechanical properties combining high strength and large ductility. Simultaneous enhancement of strength and ductility in high-Mn austenitic steels is attributed to the formation of the deformation twins, which act as obstacles against dislocation glides, then resulting in an increase of flow stress and postponement of plastic instability in deformation [1–5]. This phenomenon is termed as the twinning induced plasticity (TWIP) effect [6]. On the other hand, carbon-containing high-Mn austenitic steels frequently show serrations on their stress-strain curves. In spite of significant progress in understanding the TWIP effect in high-Mn austenitic steels, the role of the serration behavior on mechanical properties, especially strain-hardening, has not yet been clarified. Serrations have been considered as a result of interactions between dislocations and solute atoms, which is called dynamic strain aging (DSA) [7–9] or Portevin–Le Chatelier (PLC) effect [10,11]. However, it is still unclear how such a nanoscale interaction between solute atoms and dislocations results in the global deformation responses of the material including serrations on stress-strain curves.

It has also been clarified recently that materials showing the serration behavior accompany with a heterogeneous deformation characterized as propagation of strain localized bands that are of-

* Corresponding authors.
E-mail addresses: hwang.sukyoung.85z@st.kyoto-u.ac.jp (S. Hwang), park.myeongheom.8r@kyoto-u.ac.jp (M.-h. Park), bai.yu.6m@kyoto-u.ac.jp (Y. Bai), nobuhiro-tsuji@mtl.kyoto-u.ac.jp (N. Tsuji).

https://doi.org/10.1016/j.actamat.2020.116543

ten called PLC bands. The propagation of PLC bands was confirmed by using either infrared (IR) thermography or digital image correlation (DIC) technique applied during tensile deformation [12–18]. However, the macroscopic serration behavior and the local PLC banding were investigated separately in most of previous studies, and the correlation between them was not yet understood in the previous papers [12,13,15,17,18]. Recently, a few studies have correlated the serration behavior with the propagation of PLC bands in high-Mn steels by the use of the DIC method. Renard et al. [14] confirmed the formation and propagation of the PLC bands by measuring strain accumulation between two different points in the gage part of the tensile specimen. They also investigated the effect of strain rate and deformation temperature on the serration behavior, and showed that the serration behavior was promoted within certain range of the strain rate and the temperature. Similarly, Bian et al. [16] also found a relationship between the propagation of PLC bands and the serration behavior, and they clarified that the serration behavior was promoted within certain range of the strain rate with having negative strain rate sensitivity on flow stress. Like these studies, many researchers have reported that dynamic interaction between dislocations and carbon atoms are promoted under certain carbon contents [19], strain rates [14,16,20–23] and temperatures [14,21,23], leading to the characteristic serration behavior. However, the achievements so far have been mainly focused on the deformation variables under which serrations happen, and little discussion has been done on the nature of serrations and their role on global mechanical properties of materials. Some researchers have found that the serration behavior corresponded to PLC banding [14,16], but their detailed correlation is still unclear.

One of the biggest hurdle for investigating the serration behavior has been how to evaluate deformation localization in tensile tests, which cannot be measured by conventional methods like extensometer or contact strain gages that can only measure average strains of the whole specimen. The DIC technique has been introduced recently to quantify local strain distributions in deformation of various metals and alloys [14–18,24]. In the DIC method, displacements of different positions in the material are measured during the deformation. Local displacements of patterns set on the surface of the tensile specimen are tracked, which enables the quantitative evaluation of local strain distributions during the deformation. For tracking the displacements of different positions, speckle patterns are covered on the surface of the material, or the microstructure contrast itself is used as markers. By applying the DIC method, it has been quantitatively clarified, for example, how martensitic transformation in a ultrafine grained metastable austenitic steel occurred in a heterogeneous manner, i.e., in the form of Lüders deformation, during tensile deformation, which was the key to realizing ultra-high strength and large ductility of the material [24]. As mentioned in the former paragraph, propagation of PLC bands in the materials showing serration behavior has been also analyzed by the DIC method [14–18]. However, the role of PLC bands on the global deformation of materials is still unclear.

In-situ X-ray diffraction (XRD) measurement is another powerful method to understand a real-time evolution of material parameters, such as lattice strain and dislocation density, during deformation. Adachi et al. [25] investigated the grain size dependence on the evolution of dislocation density during tensile deformation in a commercial purity Al by the use of an *in-situ* synchrotron XRD measurement, and found that the increase of dislocation density could be divided into the characteristic stages of which lengths depended on the average grain size. Zhang et al. [26] revealed a development of lattice strain and dislocation density in a Lüders band propagating in a medium-Mn steel by the aid of an *in-situ* XRD measurement. By fixing a focused X-ray beam at a certain position in the tensile specimen, heterogeneous deformation like PLC banding could be characterized by the *in-situ* XRD measurement.

The current study aims to explore the nature of serration behavior of a high-Mn steel in a mesoscopic scale. The propagation of PLC bands is analyzed by means of the state-of-the-art DIC technique and the *in-situ* synchrotron XRD measurement both applied during tensile deformation of the material, for correlating the localized deformation with the global mechanical properties including the serration behavior.

2. Experimental methods

2.1. Material

A high-Mn austenitic steel, Fe-22Mn-0.6C (wt. %), was used in the present study. The detailed chemical composition of the steel is shown in Table 1. The as-received hot-forged plate 12 mm in thickness was subjected to 4 cycles of the cold-rolling and annealing treatments we developed before [27], in order to achieve grain refinement. The thickness reduction at each cold-rolling step was 33.3%, 37.5%, 40% and 66.7%, respectively, and the final thickness of the sheet was 1 mm. The intermediate annealing between each cold-rolling step was carried out at 600°C for 0.6 ks for restoring deformability of the material. The materials were water-cooled immediately after intermediate annealing. A fine-grained specimen with an average grain size of 2.0 μm was obtained by annealing the final 1 mm thick sheet at 800°C for 0.3 ks followed by water quenching.

2.2. Microstructure observation

After the final annealing, microstructural observations were carried out on a section perpendicular to the transverse direction (TD) of the sheet using a field-emission scanning electron microscope (FE-SEM: JEOL, JSM-7100F) equipped with an electron backscattered diffraction (EBSD) operated at an accelerating voltage of 15 kV. In order to obtain mirror-like surfaces, the TD section of the sheet was mechanically polished first by the use of 1000-4000 grit-sized fine SiC papers and then electro-polished in a solution of 10 % $HClO_4 + 90$ % C_2H_6O. The mean grain size was determined by a line intercept method on EBSD images, counting high angle grain boundaries and annealing twin boundaries on the EBSD maps. Texture and phases of the observed areas were also confirmed by EBSD using a software, TSL-OIM data collection and analysis ver. 5.31.

2.3. Mechanical properties

Mechanical properties of the high-Mn steel with the mean grain size of 2.0 μm were evaluated by tensile tests at an initial strain rate of 8.3×10^{-4} s^{-1} at room temperature using a tensile testing machine (SHIMADZU, AG-100kN Xplus). Sheet-type tensile specimens with a gage length of 10 mm, gage width of 5 mm and thickness of 1 mm were cut from the cold-rolled and annealed sheet by an electrical discharge machine. The tensile direction was parallel to the rolling direction (RD) of the sheet. Tensile tests of the specimen with the mean grain size of 2.0 μm were also conducted for a DIC analysis. The dimension of the tensile specimens and condition for the *in-situ* X-ray diffraction experiments are explained in the Section 2.4.2.

2.4. Evaluation of localized deformation

2.4.1. DIC analysis

In order to evaluate distributions of local strain and strain rate in the tensile specimens during the tensile test, a DIC technique was applied. Prior to the experiment, broad surfaces of the sheet-type tensile specimens were first painted white and then covered

Table 1
Chemical composition of the high-Mn steel investigated (wt. %).

C	Si	Mn	P	S	Al	Cr	O	N	Fe
0.56	0.06	21.68	<0.004	0.007	<0.01	<0.01	<0.0011	0.0049	Bal.

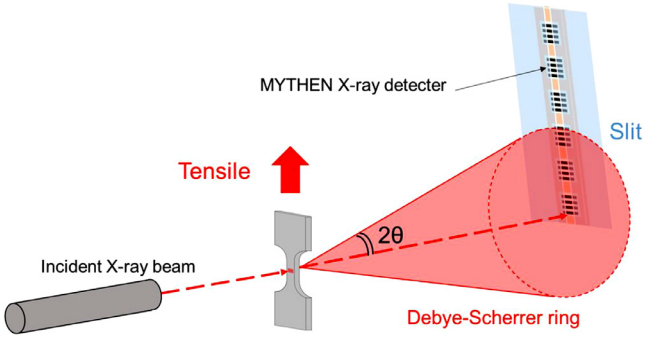

Fig. 1. Schematic illustration showing the *in-situ* XRD measurement during tensile test at SPring-8.

with randomly distributed black speckle patterns by using an airbrush. The speckle patterns were deformed together with the tensile specimens and used as markers to track displacements of different positions in the specimens. During the tensile deformation, the speckle patterns were recorded at a rate of 5 frames per second by a CCD (charge-coupled device) camera with a resolution of 2432 × 2054 pixels. Two-dimensional strain tensors at different positions were obtained by differentiating displacement vectors obtained by tracking the speckle patterns. Local strain rates at different positions were also evaluated by the use of the local strain data. From such results, distributions of strain or strain-rate in the specimen were exhibited in the form of local strain or strain-rate maps. The change of the local strain or strain-rate distributions were also expressed in movies. The recorded CCD images were analyzed by the use of Vic-2D software with a subset of 29 pixels in a square and a step size of 7 pixels, which was optimized for assessing local strains and strain rates under the given resolution of the CCD camera.

It should be noted that the global stress and the local strains (and strain rates) were obtained by different tools: the global stress of the specimen was measured from the tensile-test machine equipped with a load cell, while the local strains were evaluated from the DIC images recorded by the CCD camera as was described above. The global stress obtained from the tensile machine and the local strains obtained from the DIC analysis were synchronized by adjusting the time of macroscopic fracture.

2.4.2. In-situ *synchrotron XRD measurements*

In-situ synchrotron XRD measurements were performed for evaluating lattice strain and dislocation density during the tensile test. High energy (HE) synchrotron beam line of BL46 XU at SPring-8 of Japan Synchrotron Radiation Research Institute (JASRI) was utilized, which could provide diffraction profiles over a wide range of angles with a high resolution of time. A monochromatic synchrotron beam with an intensity of 30 keV ($\lambda = 0.0413$ nm) was used for the transmission diffraction. The time resolution for a diffraction profile was 1 second. The configuration of the *in-situ* XRD measurement during the tensile test is illustrated in Fig. 1. Sheet-type tensile specimens with a gage length of 10 mm, gage width of 3 mm and thickness of 0.5 mm were cut from the sheet having the fully recrystallized microstructure with an average grain size of 2 μm. The tensile direction was parallel to the rolling direction (RD) of the sheet. Incident beam having a size of 2.0 mm in the gage-width direction and 0.5 mm in the gage-length direction was irradiated at the center of the gage part in the tensile specimen. The direction of the incident beam was perpendicular to the tensile direction. After a precise alignment, the tensile tests with the *in-situ* XRD measurement were carried at an initial strain rate of 8.3×10^{-4} s^{-1} at room temperature. In the tensile test, the tensile specimen was elongated upward with the bottom grip part fixed. During the tensile deformation, diffraction profiles were simultaneously collected by serially-connected 6 detectors (MYTHEN X, Dectris). The diffraction peaks were fit to Voigt function using Origin Pro 2017 program, and then the peak position and full width half-maximum (FWHM) of peaks were determined. Peak positions and FWHM of (111), (200), (311) and (222) were considered for subsequent analysis.

3. Results and discussion

3.1. Microstructure before tensile test

Fig. 2(a) shows an EBSD inverse pole figure (IPF) map overlapped with an image quality (IQ) map of the specimen fabricated by the repeated cold-rolling and annealing. The microstructure was observed on a longitudinal plane perpendicular to TD of the sheet. Colors in the IPF map indicate crystallographic orientations parallel to TD, according to the key stereographic triangle inserted. High angle grain boundaries (HAGBs) and annealing twin boundaries (TBs) are drawn by black lines and red lines, respectively, on EBSD maps. The specimen showed the fully recrystallized microstructure, of which average grain size including TBs was 2.0 μm. Fig.2(b) shows a phase map together with HAGBs and TBs of the identical area of Fig. 2(a). Yellow color indicates FCC structure confirmed from the Kikuchi-line diffraction pattern obtained at each point. All areas showed yellow color, i.e., FCC structure, which proved that the specimen had an austenite single-phase structure. Fig. 2(b) also confirmed clearly that almost all grains were surrounded by HAGBs and the microstructure involved a high density of annealing TBs (39.2 % of all boundaries shown in Fig. 2(b)). (001), (011) and (111) pole figures of the specimen constructed from the EBSD result are presented in Fig. S1 in the supplementary material. All the pole figures exhibited low intensities, indicating that the specimen fabricated by the repeated cold-rolling and annealing did not have strong crystallographic texture.

3.2. Stress-strain curve and strain hardening rate curve

A nominal (engineering) stress-strain curve of the specimen with the mean grain size of 2.0 μm is shown in Fig. 3(a). The specimen showed a good combination of high strength and large ductility with a yield strength (0.2 % proof stress) of 430 MPa, tensile strength of 1136 MPa and total elongation of 69 %. Serrations were clearly observed on the stress-strain curve. Fig. 3(b) shows the strain hardening rate ($d\sigma/d\varepsilon$, blue) and true stress (σ, red) of the specimen plotted as a function of true strain (ε). The specimen maintained high strain hardening rate around 2000 MPa until the later stage of deformation. It should be noted that the strain hardening rate showed severe fluctuation from about -5000 MPa to 15000 MPa, which corresponded to the serrated flow observed on the stress-strain curve.

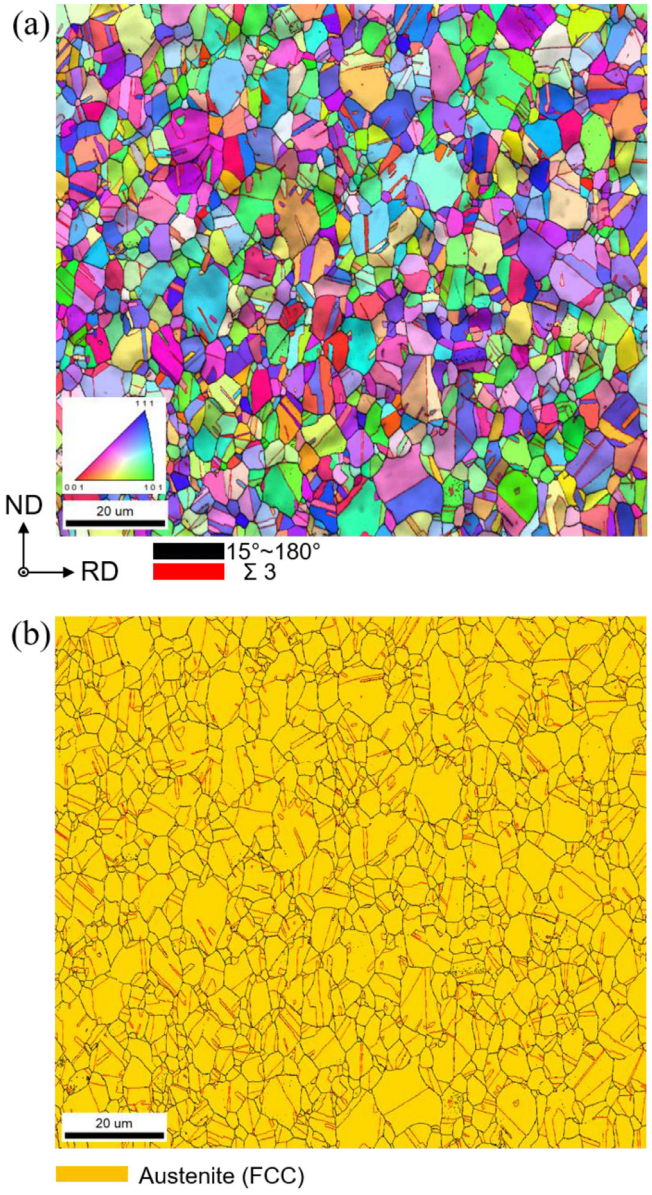

Fig. 2. EBSD images of the specimen prepared by the repeated cold-rolling and annealing. (a) EBSD IPF map + IQ map. Colors indicate crystallographic orientations parallel to TD, according to the key stereographic triangle inserted. High angle grain boundaries (HAGBs) and annealing twin boundaries (TBs) are indicated as black lines and red lines, respectively. (b) EBSD phase map with HAGBs and TBs. FCC phase is expressed in yellow color. (For interpretation of the references to color in this figure legend, the reader is referred to the web version of this article.).

3.3. Heterogeneous deformation characterized by DIC

The DIC analysis was carried out for characterizing the heterogeneity of deformation in a specimen scale. Formation and propagation of PLC bands[1] were observed in the gage part of the tensile specimen during the tensile test. It was found that the amount of strain localized within PLC bands was not so high at the early and medium stages of tensile deformation (in a range of 0.0039 ~ 0.0108), so that it was difficult to observe PLC bands on local strain maps or movies indicating the magnitude of strain in different colors using a large strain scale (like 0 ~ 0.5 in tensile strain (ε_{yy})). Hence, strain-rate maps and movies were used in the present study to exhibit or characterize the PLC bands. A movie showing the change of local strain-rate distributions during the whole tensile test up to fracture is provided as a supplementary material of this paper (Movie 1). In the movie, repetition of the formation, propagation and annihilation of PLC bands having higher local strain rates were clearly observed.

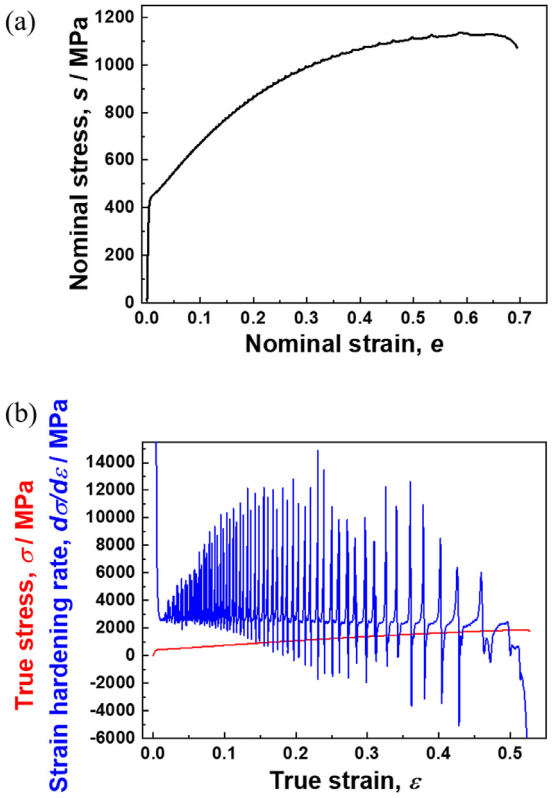

Fig. 3. (a) Engineering stress-strain curve of the specimen with a mean grain size of 2.0 μm. (b) Strain-hardening rate (blue) and true stress (red) curves plotted against true strain. (For interpretation of the references to color in this figure legend, the reader is referred to the web version of this article.).

Fig. 4 shows DIC strain-rate maps captured at different engineering tensile strains (e_{yy}) in a range from e_{yy}= 0.1193 to e_{yy}= 0.1303, which corresponded to one cycle of PLC band propagation along the whole gage length of the specimen. The numbers (1)–(9) on figures indicate the positions on the corresponding stress-strain curve shown later (Fig. 5(b)). The magnitude of local strain rate is expressed in different colors according to the key color bar inserted in Fig. 4. In (1) of Fig. 4, a PLC band (former band) having higher local strain rates propagated from the center part to the lower part of the gage was disappearing in the lower shoulder part. On the other hand, a new PLC band was nucleating at a little bit upper side of the gage center. The new PLC band propagated upward, and the propagation of the PLC band was well captured in (2), (3) and (4) of Fig. 4. The maximum strain rate within the PLC band in (2)–(4) was in a range from 0.0023 s^{-1} to 0.0027 s^{-1}, while the strain rate outside the PLC band was quite low and homogeneous (~0.0001 s^{-1}). Here, the global strain rate applied was 0.00084 s^{-1}. In (5), the band started to annihilate at the upper shoulder part, and another new band was about to nucleate at the middle of the gage part, which located slightly lower than the position where the previous band nucleated in (1). The newly nucleated band propagated downward (6, 7, 8) and was disappearing at the lower shoulder part in (9). Then, another new PLC band was nucleating at a little bit upper position of the gage center in

[1] Although it was not confirmed in the present study whether the DSA or PLC effect really happened in atomistic scale or not, the term "PLC band" is used for expressing the deformation localized bands observed.

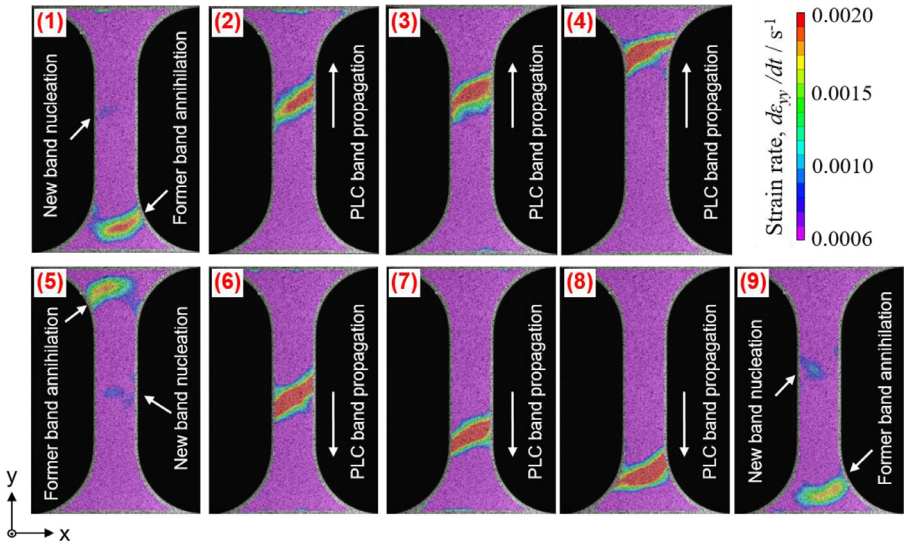

Fig. 4. DIC local strain-rate maps captured at different engineering tensile strains (e_{yy}), corresponding to one cycle of PLC band propagation through the gage part. (1) $e_{yy} = 0.1193$, (2) $e_{yy} = 0.1199$, (3) $e_{yy} = 0.1210$, (4) $e_{yy} = 0.1236$, (5) $e_{yy} = 0.1241$, (6) $e_{yy} = 0.1249$, (7) $e_{yy} = 0.1283$, (8) $e_{yy} = 0.1298$ and (9) $e_{yy} = 0.1303$, respectively. The banded regions with high strain rate shown as red color indicate the PLC bands.

(9). As can be seen in Movie 1, these showed a typical repetition of the formation, propagation and annihilation of PLC bands. The band did not necessarily form near the gage center, but often nucleated at one end of the gage part and propagated throughout the gage in one direction. Regardless of such patterns of the PLC band propagation, however, the nucleation and propagation of the band of next cycle started only after every position in the gage part was swept by the band(s) in the former cycle.

3.4. Correlation between serration behavior and PLC band propagation

Fig. 5(a) shows the change of the average strain rate in the gage part (blue curve) together with the whole nominal stress-strain curve (black curve). The average strain rate was calculated from the DIC strain-rate maps and plotted as a function of the time of the measurement which was accurately synchronized between the tensile test and the DIC analysis for the identical specimen. Corresponding nominal strains are also indicated along the upper x-axis. The average strain rate in the gage part significantly fluctuated and the time interval between each fluctuation became larger with progressing the deformation. It was noteworthy that the interval of serration peaks on the stress-strain curves also became larger with the progress of the tensile deformation, which suggested a close correlation between the fluctuation of the average strain rate and the serration behavior on the global stress-strain curve.

In order to investigate the relationship between the serration and the average strain rate in more detail, the changes of the nominal stress and the average strain rate in the experimental time from 230 s to 290 s, corresponding to the period indicated by a red broken-line square in Fig. 5(a), were magnified and exhibited in Fig. 5(b). In Fig. 5(b), thin dotted lines are drawn at the experimental times when the serration peaks appeared. It was clearly found that the serration peaks corresponded well with the local minima of the average strain rate of the gage part. When the average strain rate quickly increased from the local minimum, the flow stress quickly dropped from the serration peak.

The points (1)–(9) marked on the stress-strain curve in Fig. 5(b) corresponded to Fig. 4(1)–(9), respectively. Comparing between Figs. 5(b) and 4, at a serration peak (the point (1)) in Fig. 5(b), a former PLC band was disappearing and a new band was nucleating in Fig. 4(1). At the points (2) and (3) in Fig. 5(b) corresponding to an increase in the flow stress just after a sharp stress drop from the serration peak, the newly nucleated band was propagating upward along the gage part in the DIC maps (Fig. 4(2), (3)). At the point (4) where the flow stress was about to increase, the band was disappearing at the upper shoulder part in Fig. 4. From the point (5) to the point (8) on the stress-strain curve, annihilation, nucleation and propagation of PLC bands, which were similar to the points (1)–(4), were observed in the local strain-rate maps obtained by DIC (Fig. 4). Annihilation of the former PLC band and nucleation of the new band shown in Fig. 4(9) corresponded well again to the serration peak at the point (9) in Fig. 5(b). That is, it was clearly shown that the serration behavior appeared on the stress-strain curve perfectly corresponded with the formation, propagation and annihilation of PLC bands, i.e., localized deformation in the gage part. Thus, the fluctuation of the average strain rate in the gage part shown in Fig. 5(b) also synchronized with the behavior of PLC bands. We can conclude now that PLC banding determines the global mechanical response of the material appearing as the serration behavior on the stress-strain curve.

3.5. Changes in local strain and local strain-rate correlating to PLC band propagation

The strain rate shown and discussed in Fig. 5 was the average of the gage part obtained from the DIC data. However, the actual deformation in the gage part was heterogeneous (localized), as was shown in Fig. 4. Then, deformation behavior at a local point was analyzed from the DIC data. As represented in the image inserted in Fig. 6(a), a point in the gage part was set in the DIC maps, and changes of the local strain (ε_{yy}) and the local strain rate ($d\varepsilon_{yy}/dt$) at this point were plotted in red and blue colors, respectively, in Fig. 6(a) as a function of the experimental time. Interestingly, the strain at the analyzed point (red curve) increased in a stepwise manner, and the time interval between neighboring steps and the increment of strain at each step both increased with increasing the experimental time (i.e., the global tensile strain). The local strain rate at the analyzed point stayed in a very low value in most periods, but periodically showed sharp peaks. The peak of the local strain rate corresponded to the time at which a PLC band with high strain rates was just propagating at the analyzed point. As a result, the sudden increases in the local strain corresponded with the strain rate peaks. Both the time interval between the peaks and

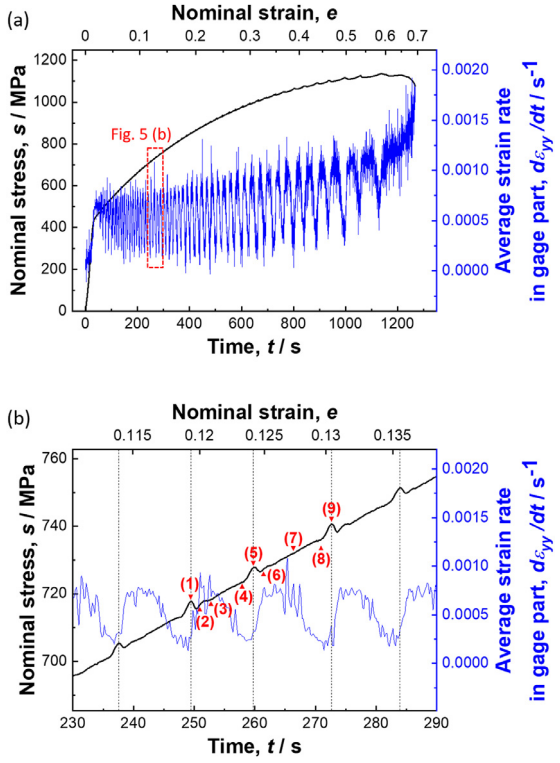

Fig. 5. (a) Change of the average strain rate in the gage part and the whole nominal stress-strain curve. The average strain rate was calculated from the DIC strain-rate maps and plotted as a function of the time of the measurement. Corresponding nominal strains are also indicated along the upper x-axis. (b) Changes of the nominal stress and the average strain rate in the experimental time range from 230 s to 290 s, indicated by a red-dashed square in Fig. 5(a). Thin dotted lines are drawn at the experimental times when the serration peaks appeared. The points (1)–(9) marked by red triangles on the stress-strain curve correspond to the DIC images shown in Fig. 4(1)–(9), respectively. (For interpretation of the references to color in this figure legend, the reader is referred to the web version of this article.).

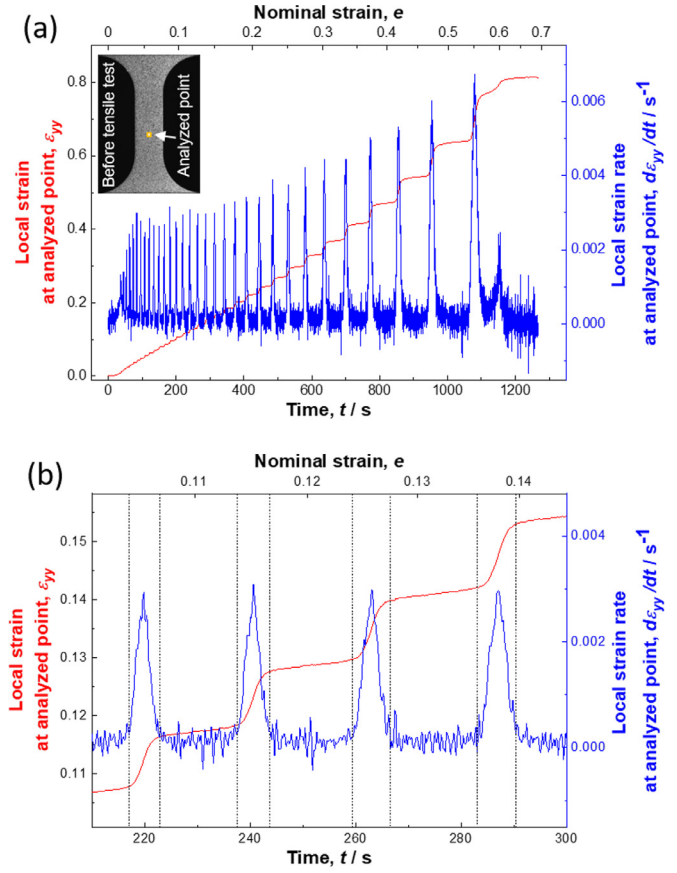

Fig. 6. (a) Changes of the local strain (red) and strain rate (blue) at a certain point set in the gage part of the DIC maps, plotted as a function of experimental time. Corresponding global nominal strain is also indicated. (b) Enlarged profiles of the local strain (red) and strain rate (blue) from 210 s to 300 s of the experimental time. The time areas of the local strain-rate peaks are distinguished by black-dashed lines. (For interpretation of the references to color in this figure legend, the reader is referred to the web version of this article.).

the maximum strain rate at the peak increased with increasing the experimental time (the tensile strain).

In order to investigate the development of the local strain and the local strain rate with the experimental time in more detail, the graph in a range from 210 s to 300 s of the experimental time was enlarged in Fig. 6(b). The time ranges of the local strain-rate peaks, which corresponded to the durations when each PLC band was passing through the analyzed point, are distinguished by black-dashed lines in Fig. 6(b). It was clearly shown that the sudden increases in the local strain perfectly coincided with the short durations of the strain-rate peaks, which meant that the strain at a certain local point increased drastically when a PLC band was passing through the point. On the other hand, increases of the local strain at the analyzed point between neighboring steps in the red curve of Fig. 6(b) were quite small, during which no PLC band was overlapped at the analyzed point. The results clearly demonstrated that most of the plastic deformation within the gage part of the tensile specimen was given within the PLC bands

3.6. Development of plastic deformation within the gage part

Features of the localized deformation (PLC banding) in the present 22Mn-0.6C steel specimen and its correlation to the serration behavior on the global stress-strain curve were demonstrated above. Here we would like to show how plastic deformation develops within the gage part of the 22Mn-0.6C specimen, again by the use of the DIC analysis. Fig. 7 shows DIC local strain maps demonstrating changes of local strain distributions (ε_{yy}) within the gage part during the deformation period from (1) to (9) shown in Figs. 4 and 5(b). Local strain maps of Fig. 7(1)–(9) corresponded to one cycle of nucleation, propagation and annihilation of PLC bands shown in Fig. 4(1)–(9), respectively. Corresponding movie showing local strain distributions during the whole tensile test is provided as a supplementary material of this paper (Movie 2). In order to exhibit the change of local strain distributions obviously, a small strain scale from ε_{yy}=0.11 to ε_{yy}=0.14 was used in Fig. 7, and the magnitude of local strain was expressed in different colors according to the key color bar inserted in the figure. The areas surrounded by white-dashed lines in Fig. 7 are the positions of PLC bands observed in Fig. 4. From (1) to (4) in Fig. 7, local strains in the upper side of the gage part became higher than the lower part, which corresponded to the PLC band propagation swept from the center to the upper side (Fig. 4(1)–(4)). At (5) where the PLC band annihilated in the upper shoulder part, strain distributions were heterogeneous and showed a clear contrast between the upper part with higher strains and lower part with lower strains in the gage. From (5) to (8) in Fig. 7, the strain in the lower side increased in this turn, corresponding to the downward propagation of the new PLC band from the center to the lower part. Then the strain distribution in the gage part became fairly homogeneous in (8) and (9) after one cycle of PLC band sweeping. The supplementary Movie 2 exhibited the repetition of such processes during the tensile deformation.

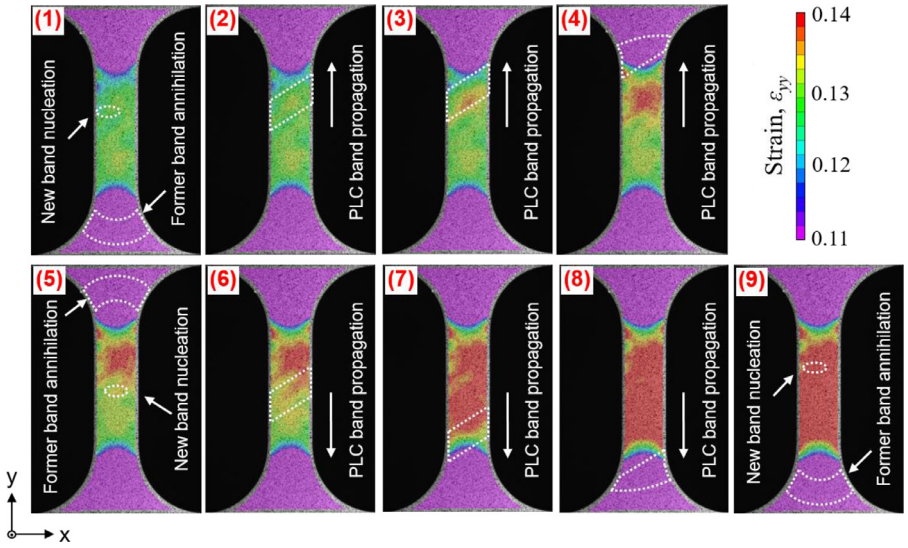

Fig. 7. DIC local strain maps captured at different engineering tensile strains (e_{yy}), corresponding to one cycle of PLC band propagation. (1) $e_{yy} = 0.1193$, (2) $e_{yy} = 0.1199$, (3) $e_{yy} = 0.1210$, (4) $e_{yy} = 0.1236$, (5) $e_{yy} = 0.1241$, (6) $e_{yy} = 0.1249$, (7) $e_{yy} = 0.1283$, (8) $e_{yy} = 0.1298$ and (9) $e_{yy} = 0.1303$, respectively. (1)–(9) exactly corresponded to the local strain-rate maps shown in Fig. 4. Positions where PLC bands were observed in corresponding strain-rate maps (Fig. 4) are marked by white-dashed lines. Magnitude of local strain was expressed in different colors according to the key color bar inserted in the figure. (For interpretation of the references to color in this figure legend, the reader is referred to the web version of this article.).

3.7. The role of PLC band on global mechanical properties revealed by in-situ synchrotron XRD measurement

The results obtained from the DIC analysis clarified that the serration behavior in the present 22Mn-0.6C steel perfectly corresponded with the heterogeneous deformation in the form of PLC banding. Next, in the current section, the *in-situ* synchrotron XRD measurement was also applied during the tensile deformation, for correlating the heterogeneous deformation clarified above with material parameters. The *in-situ* XRD measurement can reveal the changes of both dislocation densities evaluated from the peak broadening and elastic strain calculated from the peak shift, synchronizing with the physical PLC band propagation in the tensile specimen.

The results obtained from the *in-situ* XRD measurement during the tensile test are shown in Fig. 8. As was described in the Section 2.4.2, a focused X-ray beam was irradiated on a center position in the gage part of the tensile specimen. In Fig. 8(a), the whole diffraction profiles at two different stress levels of 0 MPa (before the tensile deformation) and 1000 MPa are shown on the left side, and (200) peaks at two stress levels are enlarged and shown on the right side. The (200) peak was selected for the peak-shift analysis because the (200) peak showed high intensity and its peak shift was the largest among all diffraction peaks due to the lowest elastic modulus along <100> direction in FCC metals and alloy [28]. A sharp diffraction profile of (200) plane was recognized before the deformation (at 0 MPa). Both peak broadening and peak shift were clearly found at the stress level of 1000 MPa, which were the results of accumulation of lattice defects and elastic deformation of crystal lattices, respectively. It has been reported that dislocations and planar faults contribute to the peak broadening, where diffraction angles are scattered due to local lattice distortion [29,30]. Considering that most of (both annealing and deformation) twin boundaries in FCC materials are composed of perfectly coherent $\{111\}\sum 3$ CSL boundaries, the lattice distortion produced by twin boundaries is thought to be small except for the areas near remaining leading partial dislocations or incoherent portions of twin boundaries. Balogh, Ribárik, and Ungára [30] simulated the diffraction profile of nanocrystalline pure copper by using convolutional multiple whole profile (CMWP) method. Based on the theoretically obtained profile functions, they fitted the experimentally obtained diffraction profile. In their simulation, intrinsic/extrinsic stacking faults and twin boundaries caused a peak broadening at the bottom part of a diffraction peak. In the present study, we calculated the dislocation density by using Williamson-Hall method, where FWHM of diffraction peaks (not the bottom part of diffraction peaks) were concerned. Therefore, the peak broadening caused by planar faults (deformation twin boundaries and stacking faults) would not be significant in determining the FWHM, so that it was assumed in the present study that the most of the peak broadening resulted from accumulated dislocations. The dislocation density (ρ) during the tensile test was calculated from the peak position and FWHM of (111), (200), (311) and (222) peaks at different experimental times by the use of the Williamson-Hall equation [31],

$$\frac{\Delta 2\theta \cos\theta}{\lambda} = \frac{0.9}{D} + 2\varepsilon \frac{\sin\theta}{\lambda} \tag{1}$$

$$\rho = 16.1\left(\frac{\varepsilon}{b}\right)^2 \tag{2}$$

where θ is the diffraction angle of a peak, $\Delta 2\theta$ is FWHM of the peak, λ is the wavelength of the incident X-ray beam (0.0413 nm), D is a crystallite size, ε is a heterogeneous strain, and b is the magnitude of Burgers vector (0.2552 nm in the present material), respectively. From the Eq. (1), when taking $2\frac{\sin\theta}{\lambda}$ as the x-axis and $\frac{\Delta 2\theta \cos\theta}{\lambda}$ as the y-axis, the slope of the data plots corresponds to ε. By putting ε into the Eq. (2), the dislocation density (ρ) is obtained.

In order to also evaluate the evolution of elastic strain, the change of the lattice strain during tensile deformation was calculated. The lattice strain of *hkl* plane (ε^{hkl}) under loading is calculated from the change in the interval of the lattice plane corresponding to the concerning diffraction peak, as:

$$\varepsilon^{hkl} = \frac{d^{hkl} - d_0^{hkl}}{d_0^{hkl}} \tag{3}$$

where d^{hkl} is the interval of *hkl* plane calculated from the *hkl* diffraction peak, and d_0^{hkl} is the initial interval of *hkl* plane under 0 MPa of tensile stress. As mentioned in the previous paragraph,

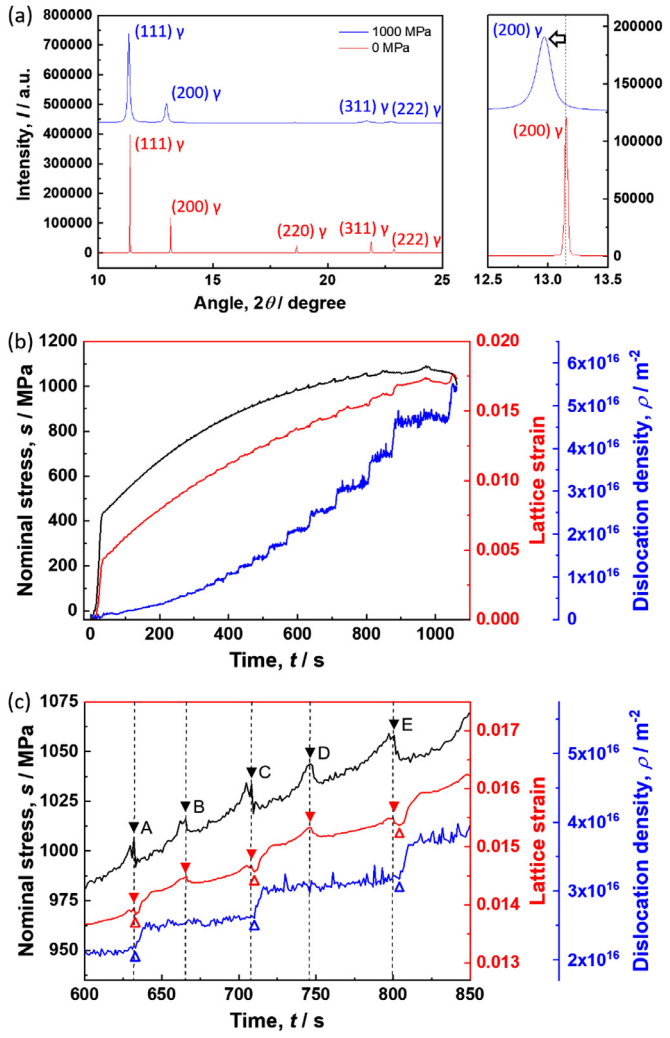

Fig. 8. (a) The whole angular diffraction profiles at 0 MPa and 1000 MPa, and enlarged (200) peaks at two stress levels are shown on the left and right side, respectively. A black dashed line in the right figure is drawn to indicate the center of the (200) peak at 0 MPa, and an arrow indicates the peak shift to lower angle at 1000 MPa. (b) The changes of nominal stress (black, left y-axis), lattice strain (red, the first right y-axis), and dislocation density (blue, the second right y-axis) are shown as a function of the experimental time. (c) Curves in the time range from 600 s to 850 s, enlarged from (b). Serration peaks are indicated by thin broken lines. Serration peaks (▼A∼▼E), peaks of lattice strain (▼), drops of lattice strain (△), and sudden increases of dislocation density (△) are indicated on the curves. (For interpretation of the references to color in this figure legend, the reader is referred to the web version of this article.).

the elastic modulus of (200) plane was the lowest in FCC metals and alloy. Therefore, by selecting the lattice strain of (200) plane (ε^{200}) for the analysis, it is possible to capture even small changes in elastic strain. The term of the lattice strain hereafter in this paper refers to the lattice strain of (200) plane.

Changes in the dislocation density and the lattice strain during tensile deformation of the present 22Mn-0.6C specimen obtained from the *in-situ* XRD measurement are shown as a function of the experimental time in Fig. 8(b), together with the nominal stress curve. It should be noted that the nominal stress showed the global deformation response in the tensile deformation, whereas the lattice strain and the dislocation density revealed the local deformation response obtained from the limited area of 0.5 mm × 0.2 mm where the XRD beam was irradiated, as was described in the Section 2.4.2.

In the lattice strain-time curve (red line) in Fig. 8(b), the lattice strain increased with the experimental time in most periods. Interestingly, however, the lattice strain dropped periodically, which indicated that periodical stress relaxation occurred at the local XRD beam position. Both the time interval between neighboring drops and the decrement of the lattice strain increased with increasing the experimental time, i.e., with the progress of the tensile deformation.

The dislocation density-time curve (blue line) in Fig. 8(b) did not show a continuous increase, but increased in a stepwise manner. During the most periods, the dislocation density at the XRD beam position did not increase significantly, but it suddenly increased at certain experimental times. In addition, both the time interval between neighboring steps increases and the increment of dislocation density at each step increased with increasing the experimental time, i.e., with the progress of the tensile deformation. The dislocation density increased up to 5 $\times 10^{16}$ m^{-2} till the macroscopic fracture. The high dislocation density might be overestimated somehow, because the peak broadening was evaluated, considering only contribution from dislocations as was described above.

In order to look into the discontinuous changes in the lattice strain and the dislocation density at the XRD beam position, the graph in a time range from 600 s to 850 s is enlarged in Fig. 8(c). Thin broken lines are drawn in Fig. 8(c) at the experimental times when serration peaks appeared on the flow stress curve (black). Different marks are used to show the positions of serration peaks (▼A∼▼E), peaks of the lattice strain (▼), drops of the lattice strain (△), and sudden increases of the dislocation density (△), respectively. On the lattice strain curve (red) in Fig. 8(c), the peaks of the lattice strain (▼) coincided well with the serration peaks (▼A∼▼E). As was explained in the Section 3.4 (Figs. 4 and 5), the serration peak appeared when PLC bands disappeared from the gage part. In addition, we figured out in the Section 3.5 (Figs. 4 and 6) that most of the plastic deformation was given within the PLC bands. Therefore, at the serration peaks when PLC bands disappeared, the whole gage part of the tensile specimen was considered to be deformed more elastically with small amounts of plastic deformation. This is the reason why the lattice (elastic) strain at the local XRD beam position showed the peaks (▼) at the same timing of the serration peaks (▼).

On the lattice strain curve (red) and the dislocation density curve (blue) in Fig. 8(c), the drops of the lattice strain (△) and the sudden increases of the dislocation density (△) synchronized to each other. Interestingly, the drops (with local minima) of the lattice strain (△) were found only after the serration peaks of ▼A, ▼C, and ▼E, but the drops (with local minima) of the lattice strain did not appear after the serration peaks of ▼B and ▼D. As was mentioned in the Section 3.3 (Fig. 4), the PLC bands in the present high-Mn steel sometimes formed near the gage center, propagated upward or downward, and disappeared at one side of shoulder part. Then new PLC bands nucleated at the center, propagated to the opposite direction of the former PLC band (downward or upward), and disappeared. It should be noted that the tensile specimen used in the present *in-situ* XRD measurement was elongated upward with its bottom grip part fixed, while the XRD beam position was fixed. In the experimental time range from 600 s to 850 s shown in Fig. 8(c), the tensile specimen was already elongated much, so that the XRD beam position was located in the lower half of the gage part. In this time range, the PLC band nucleated from the center and propagated upward never passed through the XRD beam position, but the next PLC band nucleated from the center and propagated downward passed through the beam position. Therefore, the drops of the lattice strain (△) and the sudden increases of the dislocation density (△) observed at every other serration peak (i.e., after ▼A, ▼C, and ▼E) are considered to correspond

to the PLC bands nucleated at the center and propagated downward that can pass through the XRD beam position located at a relatively lower part of the gage. That is, the drops of the lattice strain (△) correspond to the passage of PLC bands on the beam position. Since plastic deformation is localized within the PLC band, the passage of the PLC band relaxes elastic stress, resulting in the drop of the lattice (elastic) strain at the X-ray beam position by plastic deformation. In the time range of 600 s to 850 s in Fig. 8(c), the contribution of deformation twinning to tensile strain was calculated to be smaller than 16.3 %, as is shown in the supplementary material of this paper. Even though deformation twins somehow contribute to plastic deformation as an extra deformation mechanism, the tensile strain within the PLC band is considered to be given mostly by glides of many dislocations, resulting in the sudden increase of the dislocation density (△) at the X-ray beam position. The synchronized changes of the flow stress, lattice strain, and dislocation density found in Fig. 8(c) could be consistently understood in such a way.

The results obtained from the *in-situ* synchrotron XRD diffraction during the tensile test could give us the changes of material parameters in the local X-ray beam position, which consistently synchronized with the passage of the PLC band as well as the serration on the macroscopic flow stress curve. It is noteworthy that the dislocation density at the beam position significantly increased around the drops of the lattice strain (△), i.e., the passage of PLC bands, as shown in Fig. 8(c). This suggests that a large strain-hardening by an increase of the dislocation density locally occurs within the propagating PLC band, and it corresponds to the period between serration peaks (i.e., the local stress maxima) on the global stress-strain curve. The quick strain-hardening (i.e., the quick increase in the local dislocation density right after △) results in the large increases of the local lattice strain right after △ at A, C, and E in Fig. 8(c), because the local region becomes more difficult to be plastically deformed by hardening.

3.8. Correlation between global stress-strain curve (serrations) and localized deformation (PLC banding)

We have clarified in the present study that the serration behavior on the global stress-strain curve in the high-Mn austenitic steel perfectly corresponds to the local heterogeneous deformation characterized by the formation, propagation and annihilation of PLC bands. In addition, we have succeeded in correlating the heterogeneous deformation in a mesoscopic scale with the local material parameters, i.e., the dislocation density and the lattice strain in the beam position. In the current section, we summarize all the results obtained and schematically illustrate how the localized deformation induced by PLC banding develops the global work-hardening.

Fig. 9(a) schematically illustrates an enlarged stress-strain curve including three serration peaks. Nine representative stages (①–⑨) are indicated on the schematic stress-strain curve in Fig. 9(a). PLC banding in the tensile specimen, and corresponding evolutions of elastic and plastic strains at the deformation stages ①–⑨ are illustrated in Fig. 9(b). Just before the stage ①, there is no PLC band in the gage part, so that the plastic deformation is suppressed and the elastic strain quickly increases to form a serration peak. At the stage ① corresponding to the serration peak, a new PLC band nucleates near the gage center, so that elastic strain in the whole gage part of the tensile specimen decreased by plastic accommodation, leading to a stress drop in the stress-strain curve, as was observed in Fig. 8(c). Elastic strain within the nucleating PLC band starts to be furthermore relaxed while the plastic strain starts to increase. At the stage ② just after the stress drop on the stress-strain curve, the PLC band starts to propagate to the right direction. At this stage, a significant relaxation of elastic strain (thus stress) and an increase of plastic strain occur inside the PLC band, as was observed in Figs. 8(c) and 6(b), respectively. At the stage ③, the PLC band continues to propagate, and the area the PLC band already swept (yellow-colored region) has been work-hardened since a large number of dislocations are activated and accumulated, as was shown in Fig. 8(c). Because of this work-hardening, the elastic strain in the yellow region should be somehow larger than that in the left-side region where the PLC band has not yet swept. Meanwhile, the plastic strain remains almost constant in the area the PLC band has swept (yellow-colored region). At the stage ④, the PLC band has finished propagating the right half of the gage part and is disappearing at the right shoulder part. As a result, the distribution of plastic strain is heterogeneous and the right half of the gage part is more strain-hardened than the left half, as was shown in Fig. 7. From the stage ④ to ⑤ where no PLC band exists within the gage part, the plastic deformation of the specimen is greatly suppressed and the elastic deformation becomes dominant in the whole gage part, so that the flow stress of the material quickly increases to form a serration peak on the stress-strain curve. It should be noted that the slope of the stress-strain curve just before the serration peak was measured to be 5 GPa ∼ 13 GPa, which was much smaller than the Young's modulus of the present material (116 GPa). This indicates that the material still deforms plastically from the stage ④ to ⑤ even with no PLC band in the gage part. The elastic strain in the right half of the gage would be somehow higher than that in the left half, because the right half is more strain-hardened. At the stage ⑤, a new PLC band nucleates near the center, probably due to the imbalance of the plastic and elastic strains (so that the imbalance of the local stress) between the right half and left half of the gage section. The newly nucleated PLC band propagates to the left direction (to the softer region) in this turn at the stages ⑥ and ⑦. With the PLC band sweeping the left half, the plastic and elastic strains in the whole gage part becomes uniform (⑧). Then, the PLC band disappears at the left shoulder part, elastic strain in the specimen increases to form another serration peak, and a new PLC band nucleates somewhere (⑨) leading to the stress drop. By the repetition of the processes from ① to ⑧ (corresponding to one cycle of the PLC banding), the global deformation of the present material proceeds.

In the present study, we clarified the mesoscopic nature of the serration behavior in the 22Mn-0.6C austenitic steel by the aid of the *in-situ* DIC analysis and synchrotron diffraction during tensile deformation. It was shown that the plastic (and also elastic) deformation within the gage part of the tensile specimen was quite heterogeneous, and characterized by the nucleation, propagation and annihilation of the PLC bands where plastic deformation is localized. Interestingly, the serrations appearing on the global stress-strain curve, which expressed averaged deformation of the specimen totally corresponded with the localized deformation behavior, i.e., PLC banding. The characteristics of the shape of serrations, and the changes in the local lattice (elastic) strain and the dislocation density were all consistently explained by the PLC banding.

Atomistic mechanisms of the localized deformation were not clarified in the present study and further studies are necessary to clarify the nature of DSA accompanying with serrations. However, if the serration behavior is caused by DSA as has been believed, the current results suggest that dynamic interaction between dislocations and solute atoms change depending on the location with the propagation of PLC bands. Although deformation twinning can be another deformation mechanism, the contribution of twinning to plastic deformation is considered to be fairly smaller than that by dislocation slips, as was discussed in the Section 3.7. Furthermore, it is difficult to imagine that deformation twinning induces PLC banding, i.e., nucleation, propagation and annihilation of deformation localized bands observed in the present study. The quick increase of the local dislocation density within the PLC bands should be associated with the localized deformation at higher strain rates

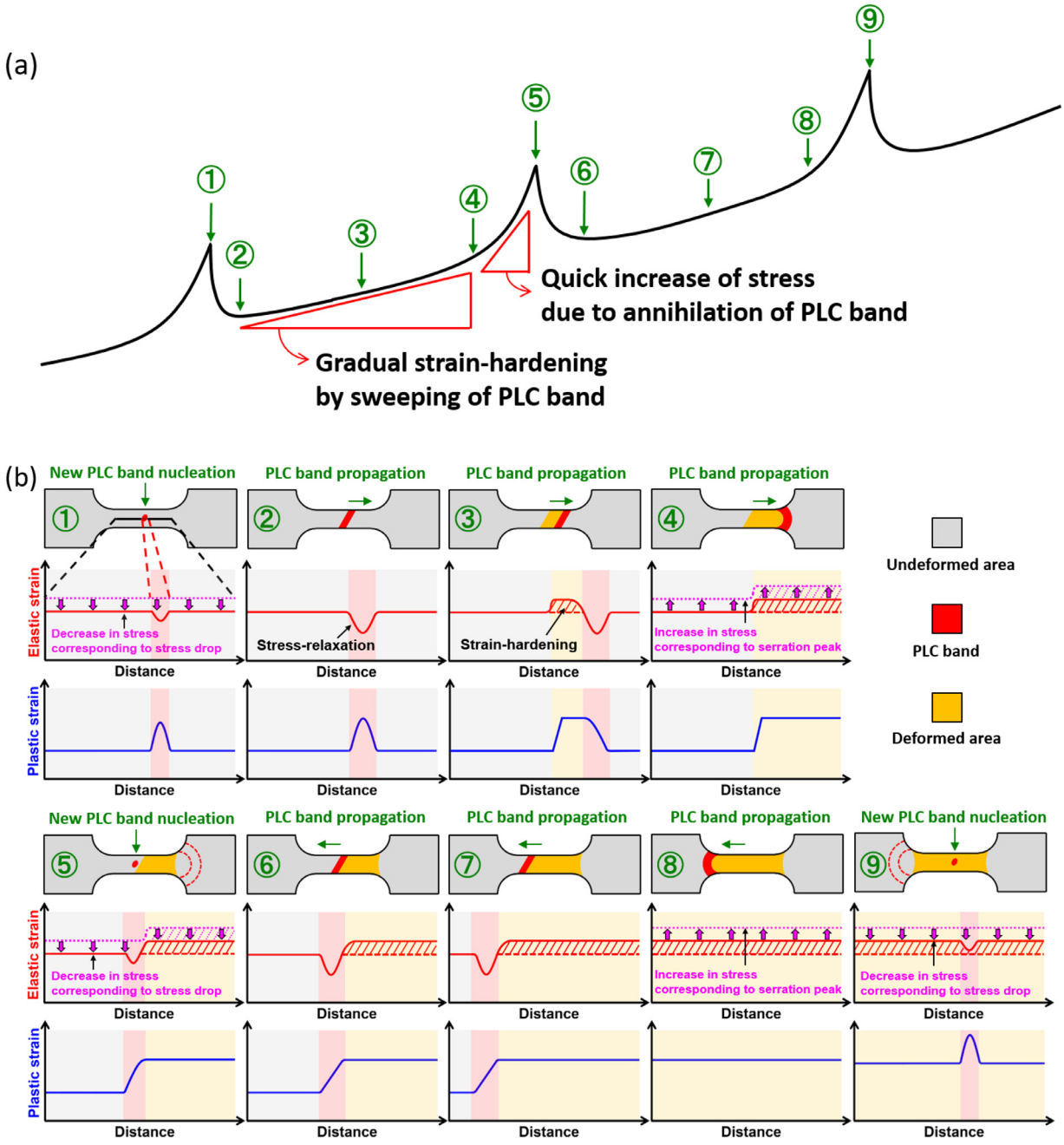

Fig. 9. Schematic illustrations summarizing the correlation between the macroscopic serration behavior and the mesoscopic localized deformation clarified in the present study. Slopes of the stress-strain curve (i.e., strain hardening) are roughly indicated by red triangles. (a) Schematic illustration of stress-strain curve including three serration peaks. (b) Schematic illustrations showing the nucleation, propagation and annihilation of PLC bands in the gage part, and corresponding distributions of elastic and plastic strains along the gage, at different stages (①–⑨) on the stress-strain curve (a). Gray, red and yellow colored areas indicate the region with little plastic deformation, the region the PLC band is propagating, and the region the PLC band already swept, respectively. (For interpretation of the references to color in this figure legend, the reader is referred to the web version of this article.).

in the bands. It should be noted that the local strains within the PLC bands were not so much high compared to those outside the bands up to medium stages of tensile deformation, which would make the whole deformation of the material relatively stable and maintain high strain-hardening rates (Fig. 3(b)). As was shown in Fig. 6(a), however, the magnitude of strains localized in the PLC bands increased with increasing tensile strain and reached to 0.0546 ~ 0.1137 at later stage of tensile deformation, which could be the reason for the fracture with small post-uniform elongation in high-Mn TWIP steels compared with other kinds of steels and metallic materials. Yu et al. [32] reported that the post-uniform elongation in 18Mn-0.6C-(0~1.5)Al steels decreased with decreasing the Al contents. In their study, PLC band propagation was observed along the side surface of the tensile specimen of the Al-free steel, whereas the PLC band was not observed in the Al-added steels. At later stage of deformation (e=30 %) of the Al-free steel, several edge cracks formed within the PLC band. They considered that the localized strain within the PLC band caused the edge crack on the side surface of the tensile specimen, leading to fracture and the limited post-uniform elongation in the Al-free 18Mn-0.6C steel.

The serration behavior is often observed in the metallic materials having good strain-hardening abilities (so that showing both

high strength and large ductility), which include not only high-Mn steels but also Al-Mg alloys, high entropy alloys, and so on. The mesoscopic features of serrations and PLC banding which have been systematically clarified in the current study would greatly help to deepen the understanding of the nature of the PLC effect (or DSA) and would throw light on designing advanced structural metallic materials maintaining good strain-hardening ability and showing excellent mechanical properties.

4. Conclusion

The mesoscopic nature of the serration behavior in a 22Mn-0.6C steel was systematically investigated by the aid of the *in-situ* DIC technique and the *in-situ* synchrotron XRD measurement during tensile tests, and the localized deformation behavior in the form of PLC banding was correlated with the global deformation of the material. The results can be summarized as follows:

1. After 4 cycles of repeated cold-rolling and annealing process, the 22Mn-0.6C steel with a fully recrystallized microstructure having the mean grain size of 2.0 μm was obtained.
2. The material exhibited the good balance of high strength and large ductility: Yield strength was 430 MPa (0.2 % proof stress), tensile strength was 1136 MPa, and total elongation was 69 %. Serrations were observed during the tensile deformation.
3. With the aid of the DIC method, it was found that the serration behavior was the response of the formation, propagation and annihilation of PLC bands (PLC banding) in the tensile specimen. It was clarified that the plastic strain increased drastically only within the PLC band, whereas the plastic strain remained almost constant beyond the PLC band. The serration peaks corresponded to the suppression of plastic deformation due to the annihilation of PLC band within the gage part. Nucleation of a new PLC band resulted in the quick stress accommodation (stress-drop) just after the peak.
4. The *in-situ* synchrotron XRD measurement at a fixed position during the tensile test revealed that the lattice strain in the X-ray beam position increased at every serration peak, which indicated that the whole specimen was more elastically deformed due to the absence of PLC band within the gage part. The dislocation density suddenly increased when a PLC band was passing through the measurement area because plastic deformation was concentrated and a large number of dislocations were introduced within the PLC band, which corresponded to a drop of the local lattice strain (elastic strain).
5. By the repetition of such a cycle of PLC banding (i.e., the nucleation, propagation, and annihilation of PLC bands) throughout the whole tensile deformation, plastic deformation of the material gradually proceeded, resulting in the global work-hardening in the present 22Mn-0.6C steel.

Declaration of Competing Interest

The authors declare that they have no known competing financial interests or personal relationships that could have appeared to influence the work reported in this paper.

Acknowledgment

The present study was financially supported by JST CREST (JPMJCR1994), Elements Strategy Initiative for Structural Materials (ESISM, No. JPMXP0112101000), and the Grant-in-Aid for Scientific Research (S) (No. 15H05767), all through the Ministry of Education, Culture, Sports, Science and Technology (MEXT), Japan. The synchrotron radiation experiments (beam-time No. 2018B1760) at SPring-8 were performed with the approval of the Japan Synchrotron Radiation Research Institute (JASRI). The author (S.H.) has been supported by the Japanese Government Scholarship. All the supports are gratefully appreciated.

Supplementary materials

Supplementary material associated with this article can be found, in the online version, at doi:10.1016/j.actamat.2020.116543.

References

[1] D.R. Steinmetz, T. Jäpel, B. Wietbrock, P. Eisenlohr, I. Gutierrez-Urrutia, A. Saeed-Akbari, T. Hickel, F. Roters, D. Raabe, Revealing the strain-hardening behavior of twinning-induced plasticity steels: theory, simulations, experiments, Acta Mater. (2013), doi:10.1016/j.actamat.2012.09.064.
[2] S. Allain, J.P. Chateau, O. Bouaziz, S. Migot, N. Guelton, Correlations between the calculated stacking fault energy and the plasticity mechanisms in Fe-Mn-C alloys, Mater. Sci. Eng. A 387–389 (2004) 158–162, doi:10.1016/j.msea.2004.01.059.
[3] A. Dumay, J.P. Chateau, S. Allain, S. Migot, O. Bouaziz, Influence of addition elements on the stacking-fault energy and mechanical properties of an austenitic Fe-Mn-C steel, Mater. Sci. Eng. A 483–484 (2008) 184–187, doi:10.1016/j.msea.2006.12.170.
[4] B.C. De Cooman, Y. Estrin, S.K. Kim, Twinning-induced plasticity (TWIP) steels, Acta Mater. (2018), doi:10.1016/j.actamat.2017.06.046.
[5] O. Bouaziz, S. Allain, C.P. Scott, P. Cugy, D. Barbier, High manganese austenitic twinning induced plasticity steels: a review of the microstructure properties relationships, Curr. Opin. Solid State Mater. Sci. (2011), doi:10.1016/j.cossms.2011.04.002.
[6] O. Grässel, L. Krüger, G. Frommeyer, L.W. Meyer, High strength Fe-Mn-(Al, Si) TRIP/TWIP steels development-properties-application, Int. J. Plast. 16 (2000) 1391–1409, doi:10.1016/S0749-6419(00)00015-2.
[7] D. Caillard, Dynamic strain ageing in iron alloys: the shielding effect of carbon, Acta Mater. (2016), doi:10.1016/j.actamat.2016.04.018.
[8] A. van den Beukel, Theory of the effect of dynamic strain aging on mechanical properties, Phys. Status Solidi (1975), doi:10.1002/pssa.2210300120.
[9] S.J. Lee, J. Kim, S.N. Kane, B.C. De Cooman, On the origin of dynamic strain aging in twinning-induced plasticity steels, Acta Mater. (2011), doi:10.1016/j.actamat.2011.07.040.
[10] A.H. Cottrell, LXXXVI. A note on the Portevin-Le Chatelier effect, Lond. Edinb. Dublin Philos. Mag. J. Sci. (1953), doi:10.1080/14786440808520347.
[11] A. Yilmaz, The Portevin-Le Chatelier effect: a review of experimental findings, Sci. Technol. Adv. Mater. (2011), doi:10.1088/1468-6996/12/6/063001.
[12] L. Chen, H.-S. Kim, S.-K. Kim, B.C. De Cooman, Localized deformation due to Portevin-LeChatelier effect in 18Mn-0.6C TWIP austenitic steel, ISIJ Int. (2007), doi:10.2355/isijinternational.47.1804.
[13] J.K. Kim, L. Chen, H.S. Kim, S.K. Kim, Y. Estrin, B.C. De Cooman, On the tensile behavior of high-manganese twinning-induced plasticity steel, Metall. Mater. Trans. A Phys. Metall. Mater. Sci. (2009), doi:10.1007/s11661-009-9992-0.
[14] K. Renard, S. Ryelandt, P.J. Jacques, Characterisation of the Portevin-Le Châtelier effect affecting an austenitic TWIP steel based on digital image correlation, Mater. Sci. Eng. A (2010), doi:10.1016/j.msea.2010.01.037.
[15] D. Canadinc, C. Efstathiou, H. Sehitoglu, On the negative strain rate sensitivity of Hadfield steel, Scr. Mater. (2008), doi:10.1016/j.scriptamat.2008.07.027.
[16] X. Bian, F. Yuan, X. Wu, Correlation between strain rate sensitivity and characteristics of Portevin-LeChâtelier bands in a twinning-induced plasticity steel, Mater. Sci. Eng. A (2017), doi:10.1016/j.msea.2017.04.078.
[17] M. Eskandari, M.R. Yadegari-Dehnavi, A. Zarei-Hanzaki, M.A. Mohtadi-Bonab, R. Basu, J.A. Szpunar, *In-situ* strain localization analysis in low density transformation-twinning induced plasticity steel using digital image correlation, Opt. Lasers Eng. (2015), doi:10.1016/j.optlaseng.2014.10.005.
[18] H. Halim, D.S. Wilkinson, M. Niewczas, The Portevin-Le Chatelier (PLC) effect and shear band formation in an AA5754 alloy, Acta Mater. (2007), doi:10.1016/j.actamat.2007.03.007.
[19] M. Koyama, T. Sawaguchi, K. Tsuzaki, Deformation twinning behavior of twinning-induced plasticity steels with different carbon concentrations–part 2: proposal of dynamic-strain-aging-assisted deformation twinning, ISIJ Int. (2015), doi:10.2355/isijinternational.isijint-2015-070.
[20] S.Y. Lee, S.I. Lee, B. Hwang, Effect of strain rate on tensile and serration behaviors of an austenitic Fe-22Mn-0.7C twinning-induced plasticity steel, Mater. Sci. Eng. A (2018), doi:10.1016/j.msea.2017.10.074.
[21] A. Saeed-Akbari, A.K. Mishra, J. Mayer, W. Bleck, Characterization and prediction of flow behavior in high-manganese twinning induced plasticity steels: part II. Jerky flow and instantaneous strain rate, Metall. Mater. Trans. A Phys. Metall. Mater. Sci. (2012), doi:10.1007/s11661-011-1070-8.
[22] Z.Y. Liang, X. Wang, W. Huang, M.X. Huang, Strain rate sensitivity and evolution of dislocations and twins in a twinning-induced plasticity steel, Acta Mater. (2015), doi:10.1016/j.actamat.2015.01.013.
[23] M. Koyama, E. Akiyama, K. Tsuzaki, Factors affecting static strain aging under stress at room temperature in a Fe-Mn-C twinning-induced plasticity steel, Tetsu-To-Hagane (2014), doi:10.2355/tetsutohagane.100.1123.
[24] S. Gao, Y. Bai, R. Zheng, Y. Tian, W. Mao, A. Shibata, N. Tsuji, Mechanism of huge Lüders-type deformation in ultrafine grained austenitic stainless steel, Scr. Mater. (2019), doi:10.1016/j.scriptamat.2018.09.007.

[25] H. Adachi, Y. Miyajima, M. Sato, N. Tsuji, Evaluation of dislocation density for 1100 aluminum with different grain size during tensile deformation by using *in-situ* X-ray diffraction technique, J. Jpn. Inst. Light Met. (2014), doi:10.2464/jilm.64.463.

[26] M. Zhang, R. Li, J. Ding, H. Chen, J.S. Park, J. Almer, Y.D. Wang, *In situ* high-energy X-ray diffraction mapping of Lüders band propagation in medium-Mn transformation-induced plasticity steels, Mater. Res. Lett. (2018), doi:10.1080/21663831.2018.1530698.

[27] Y.Z. Tian, Y. Bai, M.C. Chen, A. Shibata, D. Terada, N. Tsuji, Enhanced strength and ductility in an ultrafine-grained Fe-22Mn-0.6C austenitic steel having fully recrystallized structure, Metall. Mater. Trans. A Phys. Metall. Mater. Sci. 45 (2014) 5300–5304, doi:10.1007/s11661-014-2552-2.

[28] M.R. Daymond, M.A.M. Bourke, R.B. Von Dreele, B. Clausen, T. Lorentzen, Use of Rietveld refinement for elastic macrostrain determination and for evaluation of plastic strain history from diffraction spectra, J. Appl. Phys. (1997), doi:10.1063/1.365956.

[29] T.H. Simm, Peak broadening anisotropy and the contrast factor in metal alloys, Crystals (2018), doi:10.3390/cryst8050212.

[30] L. Balogh, G. Ribárik, T. Ungár, Stacking faults and twin boundaries in fcc crystals determined by X-ray diffraction profile analysis, J. Appl. Phys. (2006), doi:10.1063/1.2216195.

[31] G.K. Williamson, W.H. Hall, X-Ray broadening from filed aluminium and tungsten, Acta Metall. 1 (1) (1953) 22–31, doi:10.1016/0001-6160(53)90006-6.

[32] H.Y. Yu, S.M. Lee, J.H. Nam, S.J. Lee, D. Fabrègue, M. Heom Park, N. Tsuji, Y.K. Lee, Post-uniform elongation and tensile fracture mechanisms of Fe-18Mn-0.6C-xAl twinning-induced plasticity steels, Acta Mater. (2017), doi:10.1016/j.actamat.2017.04.011.